Accepted Manuscript

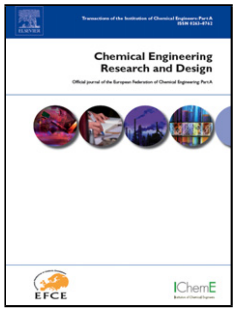

Title: Energy management of a hybrid system based on wind-solar power sources and bioethanol

Authors: <ce:author id="aut0005"> Diego Feroldi<ce:author id="aut0010"> Lucas Nieto Degliuomini<ce:author id="aut0015"> Marta Basualdo

PII: S0263-8762(13)00097-X
DOI: http://dx.doi.org/doi:10.1016/j.cherd.2013.03.007
Reference: CHERD 1197

To appear in:

Received date: 9-10-2012
Revised date: 14-3-2013
Accepted date: 18-3-2013

Please cite this article as: Diego Feroldi, Lucas Nieto Degliuomini, Marta Basualdo, Energy management of a hybrid system based on wind-solar power sources and bioethanol, *Chemical Engineering Research and Design* (2013), http://dx.doi.org/10.1016/j.cherd.2013.03.007

Research Highlights

- A new concept of multiple power sources to ensure a sustainable power supply.
- Use of wind-solar power sources to improve the reforming efficiency.
- A methodology of optimal sizing using Genetic Algorithms and historical weather data.
- The bioethanol processor allows decreasing the sizing of the other components.

Energy management of a hybrid system based on wind-solar power sources and bioethanol

Diego Feroldi[a,1,*], Lucas Nieto Degliuomini[a], Marta Basualdo[a,2]

[a] *Computer Aided Process Engineering Group (CAPEG). French-Argentine International Center for Information and Systems Sciences (CIFASIS-CONICET-UNR-AMU), 27 de Febrero 210 bis, (S2000EZP) Rosario, Argentina. TE: +54-341-4237248-304, Fax: +54-341-482-1772*

Abstract

This work presents an Energy Management Strategy (EMS) for a sustainable hybrid system. It is based on wind-solar energy and bioethanol. The bioethanol reformer produces hydrogen with sufficient quality to feed a PEM fuel cell system, which can supply the load together with the wind-solar sources. The new concept consists on having multiple power sources to supply the load where the necessary heating for the bioethanol reforming reaction can be provided by the the wind-solar sources to enhance the efficiency of the hydrogen production. An optimal sizing methodology based on genetic algorithms to design this stand-alone system is proposed. The developed model allows testing the potentiality of the proposed EMS under different scenarios of load demands using historical climate data over a period of one year. Then, the system is tested using several load scenarios to validate the proposed methodology.

Keywords: Energy management strategy, Renewable energy sources, Bioethanol, PEM fuel cells, Sustainability, Stand-alone power systems, System sizing

1. Introduction

The new technologies of energy production from renewable sources, like solar or wind energy and biofuels, are receiving much attention worldwide since the burning of fossil fuels must be replaced soon. Fossil fuels have low efficiency and high level of emissions that contribute to global warming with devastating consequences for the environment. Furthermore, it is expected a fuel shortage for the next decades.

Renewable energy sources have a great number of advantages including sustainability, reduction of carbon dioxide or other chemical pollutants and economic benefits. However, because of the intermittent nature of many renewable resources, hybrid combinations of two or more power generation technologies, along with energy storage, are necessary to improve the system sustainability. For example, wind and solar resources

*Corresponding author
Email address: feroldi@cifasis-conicet.gov.ar (Diego Feroldi)
[1] Also with Universidad Nacional de Rosario – FCEIA-DCC, Pellegrini 250, (S2000BTP) Rosario, Argentina
[2] Also with Universidad Tecnológica Nacional – FRRo, Zeballos 1341, (S2000BQA) Rosario, Argentina

in a given area can be complementary in a certain period of time (Nehrir et al., 2011). Although hybrid solar-wind energy systems reduce the energy storage requirements, the addition of some energy storage system is required in any case to guarantee that the load requirements are completely satisfied. The use of energy storage systems (e.g., different types of batteries, supercapacitors, etc.) is growing but including energy storage for extended periods of time may not be feasible. Therefore, the use of a back-up system as well as an energy storage system is necessary to achieve a reliable operation despite of the atmospheric conditions. Fuel cells together with a bioethanol reformer can offer a environment friendly and reliable supply of electricity to support load demand the for long periods.

In this work, a new concept of renewable energy system (RES) is introduced. The innovative idea is to use the hydrogen from bioethanol reforming to enhance the source energy from solar and wind power when these two sources are not capable to satisfied the load demand. This is performed through the use of a PEM fuel cell, which is feed with hydrogen from the reforming process. In turn, another innovative idea is to use part of the remaining energy of wind and solar power in the bioethanol reforming process, which increases the efficiency of that process as it is shown. Therefore, hydrogen production from bioethanol with a more efficient use of the raw material is accomplished, taking advantage of the available renewable energy sources.

The topology of the proposed system is shown in Fig. 1. This figure shows how the load power can be supplied by the wind turbine and the PV array. Hybridization between wind and solar energies has been reported in several works (Kellogg et al., 1998; Chedid et al., 1998; Borowy and Salameh, 1996; Koutroulis et al., 2006; Yang et al., 2008; Ekren and Ekren, 2008). This type of hybrid power generation systems is suitable for stand-alone applications (e.g., residential household) because of the complementary nature of wind and solar energies but also for grid-linked applications. A recent review on hybrid renewable energy systems for power generation in stand-alone applications is given in (Bajpai and Dash, 2012). Besides, another review about optimum sizing of stand-alone hybrid solar-wind power generation systems is given in (Zhou et al., 2010). Hybridization between fuel cells and solar energy has been reported in (Hwang et al., 2009) where it is considered a photovoltaic (PV) cell as the main power source using the remaining power to operate an electrolyzer that produces hydrogen from water. The hydrogen is stored in a pressurized tank and consumed by a fuel cell when extra power is required by the load. Furthermore, in (Thounthong et al., 2011) a hybrid energy system that uses renewable energy from solar cells, fuel cells and supercapacitors is proposed with an EMS based on the flatness properties of the system. Other authors, such as (Z'Graggen et al., 2008), have considered the use of concentrated solar radiation (energy source with high temperature) to produce hydrogen by steam gasification of carbonaceous materials. Additionally, a hybrid wind/PV/fuel cell alternative energy system for stand-alone applications has also been reported in (Wang and Nehrir, 2008; Nelson et al., 2006) where wind and solar energies are the primary power sources and a fuel cell-electrolyzer combination is used as a backup and a long-term storage system.

In Fig. 1 can be seen that the fuel cell system can also provide power to de DC bus when necessary.

Polymer Electrolyte Membrane (PEM) fuel cells are an excellent alternative for the production of electricity because the high efficiency compared to other technologies (e.g., internal combustion engines) and, basically, the only local emissions are water and heat. In addition, PEM fuel cells have the advantage over other types of fuel cells to work at relatively low temperatures, which makes them good candidates to work in numerous applications, including stationary power generation, automotive applications and portable electronics. Several works use a PEM fuel cell as a back-up unit together with renewable sources. In (Erdinc and Uzunoglu, 2011, 2012a; Bilodeau and Agbossou, 2006; Ipsakis et al., 2009) it is used wind and solar energy to supply the load while the excess energy produced by the sources is stored in hydrogen by using an electrolyser. This hydrogen is converted into electricity with a fuel cell when the weather conditions are unfavorable. A similar approach is presented in (Zhou et al., 2008) but without wind energy. On the other hand, the same approach is presented in (Del Real et al., 2009) but using wind energy as main energy source. Another approach of a photovoltaic/wind/fuel cell system for stand-alone applications is presented in (Eroglu et al., 2011). In this approach there is no electrolyzer for hydrogen production.

PEM fuel cells need to be fed with high-purity hydrogen to prevent degradation of the catalyst (Larminie and Dicks, 2003). However, despite its abundance in nature, hydrogen is not available in a pure form. Therefore, some processes are necessary to obtain hydrogen with sufficient quality. As it was mentioned, one alternative for hydrogen production is from electrolysis. Another interesting alternative is from ethanol. The advantages of ethanol, compared with other raw materials, are its high hydrogen content, availability, low toxicity and safety of storage and handling. In addition, ethanol can be produced by fermentation of biomass sources such as agricultural residues, forestry, livestock and urban organic. The ethanol produced in this way is called bioethanol (Basualdo et al., 2011).

The most usual methods of obtaining hydrogen from bioethanol are catalytic partial oxidation and steam reforming. The latter method is used in this work because it achieves high concentration of hydrogen required to feed a PEM fuel cell system. There is considerable research about the reaction pathways of bioethanol steam reforming. An extensive review about different technologies of integrated fuel processors for fuel cell applications is given in (Qi et al., 2007). However, this type of process requires external heating to complete the reforming reaction. A solution to this necessity was reported in (Basualdo et al., 2011), which involves burning a portion of bioethanol in a separate reactor and to provide the reaction heat from the obtained gases. However, this solution has a negative impact on system efficiency due to the extra consumption of bioethanol.

In order to avoid this situation, renewable energy sources can be used to reduce the oxidation of fresh ethanol to obtain the required heat (Degliuomini et al., 2012b). This paper proposes to use the wind-solar energy, which provides electricity to a heating system in the bioethanol reformer. However, these power sources have a high natural variability. For example, wind power can change very abruptly due to sudden gusts of wind, making it necessary to include an energy storage system, such as a battery bank, acting as a

buffer to cover the energy balance.

In this context, an Energy Management Strategy (EMS) is necessary for the correct operation of the energy subsystems, in order to meet the load demands. The EMS is an algorithm capable of commanding in real time the energy sources involved in order to meet the load requirements, while reducing consumption (Feroldi et al., 2009). Different approaches for addressing EMS in hybrid systems with multiple renewable energy sources are found in literature, depending on whether the application is stand-alone or grid-connected. In the first category, which is the case covered here, different approaches can be found such as supervisory control switching between operation modes (Valenciaga and Puleston, 2005; Degliuomini et al., 2012a) or supervisory predictive control based on model predictive control (Qi et al., 2011). A stand-alone PV-H_2 system with a double hysteresis control scheme is in (Zhou et al., 2008). Three EMS based on switching between different modes are presented and compared in (Ipsakis et al., 2009), applied to a stand-alone power system based on a PV array and wind generators that stores the excessive energy in the form of hydrogen.

The organization of this paper is as follows. In Section 2 a detailed description of the power generation system is performed. Section 3 deals with the component sizing of the hybrid renewable energy system. Section 4 deals with the energy management strategy used to manage the flow of energy within the designed system. In Section 5, the obtained results are presented and discussed. Finally, in Section 6 the conclusions and future work lines for further research are stated.

2. Description of the system and modeling

The load power can be supplied by the wind turbine and the PV array. The PEM fuel cell and the battery bank can also provide power to the DC bus when necessary. It further notes that the reformer heater can be fed, at least partially, with power from the DC bus. The power from the sources can be fully sent to the load, but if required, it can be partially sent to the battery bank to be stored temporarily and used a posteriori according to the demand. The power from the sources can be also sent to the heater of the bioethanol reformer when it is necessary to turn on the PEM fuel cell. A proper energy management strategy is responsible of commanding this operation, which is explained in detail in Section 4.

The power balance in the DC bus in Fig. 1 can be expressed as follows:

$$P_L(t) = \eta_{DA}\left(\eta_{AD}P_w(t) + \eta_{DD}P_{PV}(t) + \eta_{DD}P_{FC}(t) + \eta_{DD}P_b(t) - P_h(t)\right), \quad (1)$$

where $P_w(t)$, $P_{PV}(t)$, $P_{FC}(t)$, and $P_b(t)$ are the power provided by the wind turbine, the PV array, and the fuel cell, respectively, and $P_h(t)$ is the power consumed by the heater in the reformer. The constants η_{DD}, η_{AD}, and η_{DA} are the efficiencies of the DC/DC, the AC/DC, and the DC/AC power converter, respectively. These efficiencies are assumed to be constant, being $\eta_{DD} = 0.95$ and $\eta_{AD} = \eta_{DA} = 0.9$. On the other hand, $P_b(t)$ is negative by convention when the battery bank is charging and positive when is discharging.

Due to physical and operative limitations, the power balance is subjected to the following constraints:

$$\begin{aligned} 0 &\leq P_w(t) \leq P_w^{av}(t) \\ 0 &\leq P_{PV}(t) \leq P_{PV}^{av}(t) \\ P_{FC}^{min} &\leq P_{FC}(t) \leq P_{FC}^{max} \\ P_b^{min} &\leq P_b(t) \leq P_b^{max} \end{aligned} \tag{2}$$

The interpretation of each constraint is clarified in the following subsections.

2.1. Bioethanol reformer system (BRS)

The bioethanol reformer (BRS) system consists of an ethanol steam reformer (ESR), which performs most of the conversion of bioethanol to hydrogen, followed by three water-gas shift reactors (WGS). The catalyst of the fuel cell can be damaged if the hydrogen that enters the anode contains carbon monoxide. Therefore, further processing is necessary to remove this damaging substance. Three WGS perform the hydrogen cleaning. First, there are a high-temperature reactor (HTS) followed by a low-temperature reactor (LTS), which favors the reaction equilibrium at higher rates of CO conversion. In the third reactor, a preferential oxidation of carbon monoxide (CO-Prox) is produced, which performs the oxidation of CO in CO_2. Besides, it produces undesired oxidation of H_2, so the catalyst is selected to improve the CO conversion.

In the first step to produce the decomposition of ethanol, the bioethanol is mixed with vaporized water, and then supplied to the ESR:

$$\text{(ESR)} \quad CH_3CH_2OH + 3{\cdot}H_2O \leftrightarrow 6{\cdot}H_2 + 2{\cdot}CO_2$$

The general reaction is endothermic, thus it requires a heat supply. The amount of heat necessary to supply is $\Delta H_{298}^{o} = 254.8\ kJ\,mol^{-1}$. In the present work, it is proposed to provide this heat through a heating resistor, which is supplied with energy provided by a hybrid wind-solar system and part of the energy previously stored in the batteries. When the energy available from this sources is not sufficient, the rest of the heat is supplied by a burner, which is fed with ethanol and compressed air. The heat transfer is achieved by passing the gases through the jacket of the reformer. The reaction produced in the WGS is as follows:

$$\text{(WGS)} \quad CO + H_2O \leftrightarrow CO_2 + H_2.$$

This reaction produces heat and more hydrogen.

After the two WGS, the CO levels are still too high so that the final elimination takes place in the CO-PrOx reactor, which produces CO oxidation. In this equipment, there is also the WGS reaction previously presented. Air is injected into the CO-PrOx reactor to provide oxygen with a stoichiometry excess of 100% for good selectivity and to meet the requirements of the PEM fuel cell. The plug flow reactors are modeled as 20 continuously stirred tank reactors (CSTR) connected in cascade. Figure 2 shows a schematic diagram

of the BRS. It can be seen a heat exchangers network placed among the streams, it performs the optimal integration of the hot and cold streams, thus minimizing the consumption of auxiliary services, i. e. steam and cooling water. More details on the dynamic modeling and operation of this system can be found in (Nieto et al., 2011).

2.2. PEM fuel cell system (PEMFCS)

PEM fuel cells convert chemical energy stored in hydrogen directly into electrical energy. The basic cell comprises an anode fed with hydrogen and a cathode fed by air, although actually involved in the electrochemical reaction is the oxygen content in the air input. These two electrodes are separated by an electrolyte comprising a polymeric membrane whose main characteristic is that it allows the passage of protons when the membrane is conveniently hydrated but, by contrast, is an excellent insulator for electron (Larminie and Dicks, 2003).

The basic operating principle can be summarized as follows. The hydrogen flows through the feed channels of the anode, extending through the diffusion layer and reaches the catalytic layer, which is oxidized releasing electrons and protons according to

$$2\,\mathrm{H_2} \rightarrow 4\,\mathrm{H^+} + 4\,\mathrm{e^-}.$$

The electrons cross the metal and granulate coal of the anode catalytic layer, reaching the cathode through the external circuit, while the protons are transported through the membrane to the cathode catalyst layer. At the same time, oxygen is injected in the feed channels of the cathode, which propagates through the diffusion layer to the catalytic layer where it reacts with protons and electrons generating water according to

$$\mathrm{O_2} + 4\,\mathrm{H^+} + 4\,\mathrm{e^-} \rightarrow 2\,\mathrm{H_2\,O}.$$

Therefore, the overall reaction in the fuel cell is the following:

$$2\,\mathrm{H_2} + \mathrm{O_2} \rightarrow 2\,\mathrm{H_2\,O}.$$

The cathode reaction is exothermic, where the heat released is dependent on the voltage that is directly related to efficiency.

The rate of hydrogen consumed in the electrochemical reaction in the fuel cell anode, describe by (2.2), is a function of the fuel cell current:

$$W_{H2,\,rct} = \frac{M_{H2}\,n}{2\,F}\,I_{FC}, \tag{3}$$

where $W_{H2,\,rct}$ is the rate of hydrogen reacted, $M_{H2} = 2.016 \times 10^{-3}\,kg\,mol^{-1}$ is the molar mass of oxygen, n is the number of cells in the stack, $F = 96485\,C\,mol^{-1}$ is the Faraday number, and I_{FC} is the stack current. This is the amount of hydrogen that is required to the bioethanol processor system presented in Section 2.1.

In order to produce energy, it is necessary to integrate the fuel cell with other components to form a generation system, controlling a number of variables such as temperatures, pressures and reactant flows. These components can be divided into the following subsystems, which are strongly interrelated: reactant supply (hydrogen and air), heat and temperature control, water management, power conditioning, and power management.

A generic diagram showing the interrelation between the main components of the generation system based on fuel cell, as well as the control study, based on predictive control for the correct operation of this is reported in (Basualdo et al., 2011). This generation system consisting of a PEM fuel cell with rated power of $10\,kW$, where the most relevant control loop from the point of view of efficiency is the control of the cathode air supply.

The hydrogen consumption map of a PEM fuel cell system clearly reveals a zone, below a limit power, where the efficiency is very poor meanwhile the zone above this limit power has a significant higher efficiency (Feroldi et al., 2009). Therefore, the PEM fuel cell system is operated in this advantageous zone where the efficiency is high. The maximum power is limited by the rated power, whereas the minimum must be limited to a value below which it is not suitable to operate because the parasitic load is too large, reducing the system net power:

$$P_{FC}^{min} \leq P_{FC}(t) \leq P_{FC}^{max}. \tag{4}$$

On the other hand, the fuel cell power can not be increased faster than a certain power rise rate (ΔP_{FC}^{max}) to avoid a lack of reactants and the power can not be decreased faster than a certain power fall rate (ΔP_{FC}^{min}) to prevent overpressure into the stack (Feroldi et al., 2009):

$$\Delta P_{FC}^{min} \leq \Delta P_{FC}(t) \leq \Delta P_{FC}^{max}, \tag{5}$$

where $\Delta P_{FC}(t) = P_{FC}(t) - P_{FC}(t - \Delta T)$ and ΔT is the sample time.

2.3. Wind power system

The wind power generation system comprises a wind turbine, a multipolar synchronous generator with permanent magnets, a rectifier and a DC-DC converter to connect the generator to the DC bus. The wind turbine has three blades which convert the energy of the wind into rotational forces that drives the generator. The pitch angle of the blades is variable allowing to be adjusted operating the wind turbine at its optimal performance (Borowy and Salameh, 1996). Therefore, the power extracted from the wind turbine can be maximized according to the actual wind speed in a certain range.

The mechanical power captured by a wind turbine is proportional to the swept blade area (A $[m^2]$), the air density (ρ_a), the wind velocity (v $[m\ s^{-1}]$) and the coefficient of power (C_P), which expresses the efficiency of the turbine as a function of the ratio λ defined as $\lambda = r\omega_m/v$, where r[m] is the radius of the

blades and $\omega_m[rad\ s^{-1}]$ is the speed angle of the turbine shaft (Valenciaga et al., 2000). The ratio C_p, depending on λ and the blade pitch angle β, can be expressed as (Lei et al., 2006):

$$C_p(\lambda,\,\beta) = \frac{1}{2}\left(\frac{r\,C_f}{\lambda} - 0.022\beta - 2\right) e^{-0.255\frac{r\,C_f}{\lambda}}, \tag{6}$$

where C_f is a design constant of the blades. The values of the parameters used are as follows: $\rho_a = 1.2\,kg\,m^3$, $r = 1.6\,m$, $A = 8\,m^2$, $C_f = 19.92$. Therefore, the power from a wind turbine can be expressed as follows (Valenciaga et al., 2000):

$$P_w(t) = \frac{1}{2}C_p(\lambda,\,\beta)\rho_a A v^3(t). \tag{7}$$

However, this power is only possible for a certain range of wind speeds.

The wind turbine operation can be divided into two regions: i) above a rated wind speed v_r (full load) and ii) below-rated wind speed (partial load) (Boukhezzar et al., 2007). When the load is below the rated power P_w^r, the turbine operates at variable rotor speeds, fixing the blade pitch angle. For wind speeds above the rate value, the turbine is operated at constant output power, varying the blade pitch angle (Boukhezzar and Siguerdidjane, 2005). On the other hand, the wind turbine is stopped for wind speeds below a lower limit ($v_l = 5\,m\,s^{-1}$) and above an upper limit ($v_u = 20\,m\,s^{-1}$). Therefore, on the basis of the above and (7), the available power from a wind turbine as a function of the wind speed can be expressed as follows:

$$P_w^{av}(t) = \begin{cases} 0 & \text{if} \quad v < v_l \\ \frac{1}{2}C_p(\lambda,\,\beta)\rho_a A v^3(t) & \text{if} \quad v_l \leq v \leq v_r \\ P_w^r & \text{if} \quad v_r < v \leq v_u \\ 0 & \text{if} \quad v > v_u \end{cases}. \tag{8}$$

2.4. Solar power system

The solar power system is composed of a PV cell array and a buck DC/DC power converter. In a PV array, the electromagnetic radiation of solar energy can be directly converted into electricity through photovoltaic effect. Therefore, the electric energy generated by a PV cell depends on several parameters and atmospheric conditions such as insolation and temperature. This atmospheric conditions affects significantly the performance of the PV cells. Some of the parameters affecting the performance are related with the effective area, determined by its configuration, and the particular technology.

The electric behavior of a PV cell can be modeled by a nonlinear current source connected in series with the intrinsic cell series resistance. The current provided by this equivalent nonlinear source (I_{PV} $[A]$) depends mainly on the actual insolation and the temperature (Valenciaga et al., 2001):

$$I_{PV}(t) = I_{ph}(t) - I_{rs}(t)\left(\exp\left(\frac{q\,(V_{PV}(t) + I_{PV}(t)R_s)}{A_c K T(t)}\right) - 1\right), \tag{9}$$

where I_{ph} is the generated current under a given insolation, I_{rs} is the cell reverse saturation current, V_{PV} is the voltage level on the PV panel array terminals, q is the charge of an electron, R_s is the intrinsic cell

resistance, A_c is the cell deviation from the ideal p-n junction characteristic, K is the Boltzman constant, and T is the cell temperature. The reverse saturation current and the photocurrent depend on insolation and temperature according to the following expressions:

$$I_{rs}(t) = I_{or}\left(\frac{T(t)}{T_{ref}}\right)^3 \exp\left(\frac{qE_{go}(1/T_r - 1/T(t))}{KT(t)}\right), \quad (10)$$

$$I_{ph}(t) = (I_{sc} + K_l(T(t) - T_r))\lambda(t)/100, \quad (11)$$

where I_{or} is the reverse saturation current at the reference temperature T_{ref}, E_{go} is the band-gap energy of the semiconductor used in the cell, I_{sc} is the short-circuit cell current at the reference temperature and isolation, K_l is the short-circuit current temperature coefficient and λ is the insolation in mW/cm^2. The values of these constants are given in Table 1.

A typical PV cell produces less than 2 W at 0.5 V approximately, thus the cells must be connected in series-parallel configuration on a module to produce enough power (Tsai et al., 2008). A PV array is a group of several PV modules which are electrically connected in series and parallel circuits to generate the required current and voltage. Thus, the available current for a PV array can be expressed as follows:

$$I_{PV}^{av}(t) = n_p I_{ph}(t) - n_p I_{rs}(t)\left(\exp\left(\frac{q\left(V_{PV}(t) + I_{PV}(t)R_s\right)}{n_s A_c K T(t)}\right) - 1\right), \quad (12)$$

where n_p is the number of parallel modules, and n_s is the number of cells connected in series in each parallel module (values in Table 1). Therefore, the available power generation from a PV array is

$$P_{PV}^{av}(t) = V_{PV}(t) I_{PV}^{av}(t). \quad (13)$$

As is shown in Fig. 1, the PV array is connected to the DC bus through a DC/DC buck converter, allowing to regulate the power generation. The dynamic response of the solar subsystem is determined by the operation of the DC/DC buck converter. The dynamic response of the system can be expressed through the following equations:

$$\dot{V}_{PV}(t) = \frac{1}{C}\left(I_{PV}(t) - I_o(t)\right)u(t), \quad (14)$$

$$\dot{I}_{PV}(t) = \frac{1}{L}\left(-V_b(t) + V_{PV}(t)\right)u(t), \quad (15)$$

where C and L are the capacity and inductance in the DC/DC converter, V_b is the voltage on the battery bank terminals, I_o is the current on the output terminal of the DC/DC voltage, and u is the control signal commanding the DC/DC. The control signal u is a switched signals with discrete values 0 (switch opened) and 1 (switch closed), fixed frequency, and variable duty cycle. Therefore, from (13), (14) and (15), the power supplied by the PV array to the DC bus can be expressed as follows:

$$P_{PV}(t) = P_{PV}^{av}(t)u(t). \quad (16)$$

Accordingly, $P_{PV}(t)$ can be controlled to a desired reference through the control signal $u(t)$.

2.5. Energy storage system (ESS)

The natural variability of wind-solar power, in addition to being a stand-alone application without connection to the grid, implies the need to include an energy storage system to have a reliable power supply. The energy storage system acts as a buffer to cover the energy balance, providing or absorbing energy as needed. The ESS can be implemented either by a high specific energy device such as batteries or by a high specific power device such as supercapacitors. There is also the possibility of a combined solution using batteries and supercapacitors (Henson, 2008). To meet the power objective in this application, it requires that the storage bank has high-energy capacity but also must be able to manage high peak power. Indeed, an important parameter to characterize energy storage elements is the Power/Energy ratio (P/E) defined as follows (Pede et al., 2004):

$$P/E\,[W\,Wh^{-1}] = \frac{P[W\,kg^{-1}]}{E[Wh\,kg^{-1}]}. \tag{17}$$

In this paper, we have chosen to use nickel-metal hydride (Ni-MH) batteries due to the most relevant characteristics (capacity, power, efficiency, number of load cycles, price, low toxicity) compared to other types of batteries such as lead acid or lithium ion (Li-Ion). Conventional lead-acid batteries are the least expensive for hybrid energy system applications, but they suffer from a low cycle life Nehrir et al. (2011). Different studies relate the best utility of such batteries (Liu et al. (2010), Nehrir et al. (2011)). The main characteristics of the Ni-MH battery bank are given in Table 2. According to (17) and the parameters of the battery bank, $P/E = 6.5\,W\,Wh^{-1}$, which is appropriate to provide the possible power peaks.

The battery is modeled as an equivalent circuit comprising a voltage source, which represents the open circuit voltage (V_{oc}), in series with an internal resistance (R_{int}). Therefore, the terminal voltage of the battery is $V_{bat} = V_{oc} - I_{bat}\,R_{int}$. In this model, both V_{oc} and R_{int} depend on the battery state of charge (SOC_b), which represents the remaining capacity still available to be discharged from the battery. In the model, the nonlinear interactions of V_{oc} and R_{int} depending on SOC_b are expressed as data vectors and their values are obtained by interpolating within the corresponding vector according to the current SOC_b. These vectors are based on experimental data of the manufacturer and can be obtained from the modeling tool of hybrid automation systems called ADVISOR (Johnson, 2002).

The state of charge (SOC_b) of a rechargeable battery is an important parameter as well as being a measure of the amount of available power. The SOC_b must be kept within certain limits, for example, $20\% \leq SOC_b \leq 90\%$ (Milocco and Castro, 2009), to ensure good performance and battery life. The SOC_b can be expressed as

$$SOC_b = \frac{C_b^{*,\,max} - C_b^{*,\,u}}{C_b^{*,\,max}} \cdot 100 \quad [\%], \tag{18}$$

where $C_b^{*,\,max}$ is the maximum capacity, in units of Ah, and $C_b^{*,\,u}$ is the amount of Ah already used, which can be computed as

$$C_b^{*,\,u} = \int_0^t \frac{\eta_c\,I_b}{3600}\,dt \quad [Ah], \tag{19}$$

where η_c is the charge/discharge battery coulombic efficiency, in this case $\eta_c = 0.975$, and I_b is the battery current in units of A at the current instant, being $I_b > 0$ when the battery discharges and $I_b < 0$ when it charges. The initial SOC_b is represented using a non-zero initial value of $C_b^{*,u}$.

On the other hand, the battery current is limited, I_b^{lim}. These limit depend on V_{oc} and R_{int} through the following expressions:

$$I_b^{lim} = \begin{cases} \frac{(V_{oc} - V_b^{max})}{R_{int}} & \text{during charging} \\ \frac{(V_{oc} - V_b^{min})}{R_{int}} & \text{during discharging} \end{cases}, \tag{20}$$

where V_b^{min} and V_b^{max} are the minimum and maximum allowable battery bank voltage, respectively. Additionally, I_b^{lim} depend indirectly on SOC_b through the previously mentioned nonlinear relationships. Furthermore, there is another mechanism for limiting the battery bank current in order to force a current zero when the SOC_b reaches its maximum or minimum value. Therefore, the limit battery power is $P_b^{lim}(t) = I_b^{lim}(t)V_b(t)$.

3. Component sizing of the hybrid system

Component sizing of hybrid renewable energy systems is an important topic in order to ensure the power supply to the load while being economically viable. In fact, there is a tradeoff between cost and reliability in hybrid sizing. However, in stand-alone systems, the main priority is the reliability of the system (Rajkumar et al., 2011). Therefore, the main objectives in the design process can be stated as follows: (a) achieve a reliable power supply under varying atmospheric conditions and (b) minimize the total system cost.

The power reliability analysis is an important step in the component sizing process. A reliable electrical power system can be defined as a system with sufficient power to feed the load demand during a certain period or, in other words, with a small loss of power supply probability ($LPSP$) (Yang et al., 2008). $LPSP$ is defined as the probability that the hybrid system is unable to satisfy the load demand (Yang et al., 2003). A $LPSP$ of 0 means the load is always satisfied while an $LPSP$ of 1 means that the load is never satisfied. The objective function $LPSP$ can be expressed as follows:

$$LPSP = \frac{T_{ft}}{T_t}, \tag{21}$$

where T_t is the total time of weather data used in the analysis and T_{ft} is the power failure time, which is defined as the time that the load is not satisfied:

$$T_{ft} = \sum_{t=0}^{T_t} \varphi(t)\Delta T, \tag{22}$$

where ΔT is the sample time in the discrete data, and

$$\varphi(t) = \begin{cases} 1 & \text{if} \quad P_T^{av}(t) < P_T^{req}(t) \\ 0 & \text{otherwise} \end{cases}. \tag{23}$$

Therefore, the main objective of component sizing is that $LPSP < LPSP_a$, where $LPSP_a$ is the allowed $LPSP$.

The determination of the optimal sizing can be addressed using several methods such as heuristic methods, linear programming (LP), interior point method (IPM), genetic algorithm (GA) or particle swarm optimization (PSO). Techniques like GA or PSO are specially convenient when multiple objectives are to be met, e.g., minimizing cost, maximizing system reliability and efficiency, etc. In this work, the minimization of the objective function, which takes into account the cost of the system, the maintenance cost along the time, and the reliability of the system to meet the load is implemented employing a GA. An extensive review about optimum design of hybrid renewable energy systems is given in Erdinc and Uzunoglu (2012b).

A GA is a stochastic global search method, which has been developed to imitate the evolutionary principle of natural genetics (Yang et al., 2008). They are used in several works concerning the component sizing in hybrid renewable systems like (Yang et al., 2008; Koutroulis et al., 2006; Xu et al., 2005). Although GA is a stochastic method, it is generally more robust in finding a global optimal solution than other optimization methods, specially in multi-objective problems (Yang et al., 2008).

The objective of the fitness function evaluation is expressed as follows:

$$\min_{\mathbf{x}} \{J(\mathbf{x})\} = \min_{\mathbf{x}} \{\rho C_T(\mathbf{x})\}, \tag{24}$$

where $\mathbf{x}$ is the vector of the decision variables (N_w, N_{PV}, and N_b) and ρ is a penalization term defined as follows:

$$\rho = \begin{cases} 1 & \text{if } LPSP < LPSP_a \\ \rho_p & \text{otherwise} \end{cases}, \tag{25}$$

and $\rho_p \to \infty$ is a sufficiently large constant to avoid solutions that do not meet the $LPSP$ requirement.

The total cost $C_T(\mathbf{x})$ can be expressed as

$$C_T(\mathbf{x}) = C_C(\mathbf{x}) + C_M(\mathbf{x}) + C_R(\mathbf{x}), \tag{26}$$

where $C_C(\mathbf{x})$ is the initial cost, $C_M(\mathbf{x})$ is the operation and maintenance cost over the lifetime, and $C_R(\mathbf{x})$ is the replacement cost according to the following expressions:

$$C_C(\mathbf{x}) = N_w C_{C,w} + N_{PV} C_{C,PV} + N_b C_{C,b} \tag{27}$$

$$C_M(\mathbf{x}) = T_{op}(N_w C_{M,w} + N_{PV} C_{M,PV} + N_b C_{M,b}) \tag{28}$$

$$C_R(\mathbf{x}) = T_{op}(N_w C_{R,w} + N_{PV} C_{R,PV} + N_b C_{R,b}) \tag{29}$$

where $C_{C,w}$, $C_{C,PV}$, and $C_{C,b}$ are the initial cost of one wind turbine, one PV panel and one battery, respectively; $C_{M,w}$, $C_{M,PV}$, and $C_{M,b}$ are the yearly maintenance cost of one wind turbine, one PV panel, and one battery, respectively; $C_{R,w}$, $C_{R,PV}$, and $C_{R,b}$ are the replacement cost of one wind turbine, one PV panel, and one battery, respectively; and T_{op} is the operation time.

The total available power in the DC bus is

$$P_T^{av}(t) = N_w \eta_{AD} P_{w,\,un}^{av}(t) + N_{PV} \eta_{DD} P_{PV,\,un}^{av}(t) + N_{FC} \eta_{DD} P_{FC,\,un}^{av}(t) + N_b \eta_{DD} P_{b,\,un}^{dsch}(t), \tag{30}$$

where $P_{w,\,un}^{av}(t)$ is the power generated by one wind unit, $P_{PV,\,un}^{av}(t)$ is the power generated by one solar unit, $P_{FC,\,un}^{av}(t)$ is the power generated by one PEM fuel cell module, $P_{b,\,un}^{dsch}(t)$ is the battery discharge power, N_w is the number of wind units, N_{PV} is the number of solar units, and N_b is the number of battery modules. The number of PEM fuel cell modules is $N_{FC} = 1$ because it was preferred to have a larger single stack instead of multiple stacks for operational reasons. The total power required in the DC bus is

$$P_T^{req}(t) = \frac{1}{\eta_{DA}} P_L^{req}(t) + P_h^{req}(t), \tag{31}$$

where $P_h^{req}(t)$ is the required power by the heater when the reformer-fuel cell system is operating.

For component sizing, $P_T^{av}(t)$ and $P_T^{req}(t)$ can be broken down into two different powers according to two scenarios, defined as follows.

Scenario 1 is a favorable situation when the wind-solar energy is enough to supply the load and thus the PEM fuel cell is off. Therefore,

$$P_{T,\,1}^{av}(t) = N_w \eta_{AD} P_{w,\,u}^{av}(t) + N_{PV} \eta_{DD} P_{PV,\,u}^{av}(t) + N_b \eta_{DD} P_{b,\,u}^{dsch}(t), \tag{32}$$

and

$$P_{T,\,1}^{req}(t) = \frac{1}{\eta_{DA}} P_L^{req}(t). \tag{33}$$

Oppositely, Scenario 2 is a worst-case situation when the wind-solar energy is null due to unfavorable atmospheric conditions, and the PEM fuel cell is turned on to cover the power demand. Therefore,

$$P_{T,\,2}^{av}(t) = N_{FC} \eta_{DD} P_{FC,\,u}^{av}(t) + N_b \eta_{DD} P_{b,\,u}^{dsch}(t), \tag{34}$$

and

$$P_{T,\,2}^{req}(t) = \frac{1}{\eta_{DA}} P_L^{req}(t) + P_h^{req}(t). \tag{35}$$

Therefore, the component sizing can be separated in two stages.

In the proposed design process, an optimization problem based on genetic algorithms is resolved first, according to Scenario 1. In this problem, it is determined the number of wind turbines and PV modules. Hybrid solar-wind systems usually meet load demands satisfactorily because of the complementary effect of solar radiation and wind speed. The optimal determination of the total number of photovoltaic and wind energy devices depends on the potential solar radiation and wind speed during the considered time period. If the system is designed to supply energy throughout a year, the hybrid system must be designed according to the solar and wind resources available in the same period (Yang et al., 2008). Since the solar-wind systems is the primary source, the proposed methodology sizes these systems taking into account the energy produced over a year and the energy required by the load in the same period.

In the next stage, the size of the fuel cell and the battery bank is determined according to Scenario 2. The fuel cell system is sized as a base power source to meet the average load. Therefore, the size of the battery bank is determined considering the necessary peak power to meet transitory requirements. The batteries are connected in series to give the desired nominal DC operating voltage, and they are connected in parallel to yield the necessary storage capacity. Then, the number of batteries connected in series ($N_{b,\,s}$) depends on the DC bus voltage and the nominal voltage of each individual battery (V_b^{nom}), being calculated as follows:

$$N_{b,\,s} = \frac{V_{bus}^{nom}}{V_b^{nom}}. \tag{36}$$

Therefore, the number of batteries to be connected in series is a result of a straightforward calculation. However, to determine the number of parallel battery strings ($N_{b,\,p}$), each consisting of $N_{b,\,s}$ batteries connected in series, a further analysis is necessary. This analysis considers the total capacity of the battery bank:

$$C_{b,\,T}^{*} = C_b^{*}\, N_{b,\,p}. \tag{37}$$

In order to achieve a sustainable hybrid power system, the capacity $C_{b,\,T}^{*}$ is determined to meet transitory power requirements. Specifically, $C_{b,\,T}^{*}$ is designed to cover the average load in a worst-case scenario defined as long periods without solar radiation and no-wind periods of 1 h. Once determined $N_{b,\,p}$, the total number of batteries in the bank is $N_{b,\,T} = N_{b,\,s}\, N_{b,\,p}$.

The developed methodology has been applied to design the stand-alone hybrid wind-solar system in order to supply a maximum load of 20 kW, located in the area of Rosario (Argentine) with geographical coordinates defined as latitude: 32°51'S, longitude: 60°54'W, and altitude: 25 m above sea level. The design process is performed using the historical hourly data of solar radiation (accessed from (HomerEnergy, 2012)), wind speed and ambient temperature (accessed from (Meteored, 2012)) over the year 2011, which are plotted in Fig. 3, ,4, and 5. This data is used in the sizing methodology based on GA algorithm to find the values of vector $\mathbf{x}$ that satisfies $LPSP < LPSP_a$ and, at the same time, minimizes the cost $C_T(\mathbf{x})$.

The data chosen to be the load requirement for the hybrid wind-solar system is a normally distributed random signal sampled every hour, generated with a mean of 10 kW and a standard deviation of 2.25 kW.

The values of costs used in the algorithm (shown in Table 3) are based on the costs presented in (Rajkumar et al., 2011), which are taken as a reference for this work.

For practical reasons the number of wind turbines is allowed between 0 and 2. The optimal sizing results of the hybrid system are presented in Table 4. In Fig. 6 it can be seen the variation of the cost during the GA optimization process.

4. Energy management strategy

The DC bus can be supplied with power produced by the wind turbines, the PV array, the PEM fuel cell, and the battery bank. In turn the heating resistor in the bioethanol reformer is supplied with power from the DC bus. As already mentioned, wind and solar energy sources have great variability according to the atmospheric conditions, although they are somewhat complementary. On the other hand, the inclusion of a battery bank, as the one previously described, allows to store energy temporarily in order to cover the energy balance but, most importantly, it allows to operate the wind generation system more efficiently at any time, regardless of the required load at that same moment. However, this can only be achieved within certain limits according to the constraints of the system, primarily within the operating limits of SOC_b battery bank. To overcome this drawback, in the proposed topology, the PEM fuel cell plays a crucial role to meet the demand during prolonged periods with little wind and radiation.

Therefore, it is required to define an adequate energy management strategy (EMS) to command the hybrid generation system, i.e., to determine at each instant the operation of the wind turbine, the PV array, the PEM fuel cell, and the battery bank, depending on the load requirements, the SOC_b, and the atmospheric conditions. The operation must ensure that the energy balance in (1) is met, subjected to the constraints in (2).

The available power from the wind subsystem is $P_w^{av}(t) = i_w^{av}(t)V_{bus}(t)$ according to (8), while the available power from the solar subsystem is $P_{PV}^{av}(t) = i_{PV}^{av}(t)V_{bus}(t)$ according to 13. The available currents $i_{PV}^{av}(t)$ and $i_w^{av}(t)$ are defined according the input currents to the DC-DC converters (see Fig. 1) and the respective conversion ratios. The wind turbine, solar cells and the reformer-fuel cell are usually controlled by inner regulation loops. The dynamics of these loops are much faster than those of outer control loops. Therefore, the current of each power source is considered to follow its reference perfectly (Thounthong et al., 2011).

In the proposed EMS, the main generation role is in charge of the wind subsystem while the solar subsystem plays a complementary role. The motivation for this criterion is because of the intended application is in geographical areas with wealthy wind regimes. Therefore, the first objective is that the proposed energy management strategy operates the wind turbine at its maximum power point so long as possible. Thus, the role of the solar subsystem is to reinforce the wind subsystem. Similarly, the battery bank also reinforces the wind-solar subsystems.

The EMS can be formalized using a state machine approach. State machine is a powerful tool to implement decision making algorithms. It can be used both as a development tool for approaching and solving problems and as a formal way of describing the solution for later developers and system maintainers. In the state machine concept, the system makes a transition from one state (mode) to another, provided that the condition defining the change is true. Thus, a state machine consists of state variables, which encode

its states, and events, which transforms its states. A state machine can be represented by a statechart. The statechart representing the proposed EMS is given in Fig. 7. The statechart can be defined by a tuple $\langle S, \Sigma, \delta \subseteq S \times \Sigma \times S, s_0 \rangle$ where

- $S = \{s_1, s_2, s_3, s_4, s_5\}$ is the set of all nodes in the statechart.
- $\Sigma = \{1, 2, 3, 4, 5, 6, 7, 8\}$ is the set of possible input events (see Table 5).
- δ is a function that maps states and input events to states ($\delta : S \times \Sigma \rightarrow S$), which can be expressed in the form of a state/event table (see Table 6). Note that is a prioritized table, i.e., the events are evaluated in the order shown to determine the next state.
- s_0 is the initial state, i.e., an element of S. In this case is $s_0 = s_1$.

The description of the event in the set Σ is given in Table 5. The description of each state in the set S is the following:

- State 1 (s_1): When the wind power is sufficient to satisfy the total demand, the wind subsystem operates at maximum power (point of maximum energy conversion) to satisfy the demand, and recharge the battery bank with the remaining energy, while the solar subsystem is inactive. The battery bank demands the recharge current, and becomes part of the demand.
- State 2 (s_2): When the wind subsystem is not capable of supporting the load by itself, the wind subsystem is set for maximum generation and the solar subsystem supplies the remaining power to satisfy the power balance. The battery bank is also in charging mode.
- State 3 (s_3): When the two power subsystem together are not capable to met the power requirement, they operate at their maximum energy conversion points and the battery bank supplies the remaining power to fully satisfy the load demand. Thus, in this mode, the battery bank reverts the current direction, acting as a power supplier depleting the previously stored energy (discharging mode).
- State 4 (s_4): When the battery bank SOC_b reaches the maximum limit (SOC_b^{max}), the power sources are disconnected, and the battery bank operates in mode discharging, supplying the required load.
- State 5 (s_5): When the battery bank SOC_b reaches the minimum limit (SOC_b^{min}), the PEM fuel cell and the reformer are connected. The energy required by the heather is supplied by the solar-wind subsystems. The battery bank operates in mode charging, allowing to recover the charge.

5. Results and discussion

The optimal hybrid system, designed as it was explained in Section 3, is tested with the enunciated EMS by simulation. For this purpose, a complete model of the system was implemented in Matlab/Simulink,

according to the description in Section 2. The parameters used in the EMS are presented in Table 7.

The hourly average wind speed, ambient temperature and solar insolation data for a typical day (September 19, 2011) in the mentioned location are shown in Fig. 8 and Fig. 9. The wind speed and insolation profiles are from a given day between the data set considered in the design process. The hourly temperature throughout a day is estimated using a model of temporal variation in air temperature (Campbell and Norman, 1998), which uses the maximum and minimum temperature of present, previous and next day. This model assumes that minimum temperatures normally occur just before sunrise and maximum temperatures about two hours after solar noon. On the other hand, average hourly load demand data for a typical stand-alone load is shown in Fig. 10. These data are used to test the designed hybrid system with the proposed energy management strategy. The generation and load are assumed to be linearly interpolated into each hour interval.

The hybrid system is tested with different load scenarios and also starting with different state of charge (SOC_b^{init}). First, the system is evaluated with the load profile in Fig. 10 and an initial state of charge $SOC_b^{init} = 80\%$. The power balance in the DC bus is shown in Fig. 11, the SOC_b is shown in Fig. 12, and the operation mode is shown in Fig. 13. It can be seen that the system operates almost exclusively in mode 3 and satisfactorily meets the load requirement despite during most of the time the wind-solar generation is small. The system is also evaluated with the same load profile but starting with a lower SOC_b: $SOC_b^{init} = 40\%$ (Fig. 14, 15, and 16). This demanding load profile coupled with the low SOC_b^{init} causes the system operate in mode 5 (fuel cell on).

The system is also evaluated with a lower load profile where it can be seen the operation of the battery bank in charging mode (mode 1). These results are shown in Fig. 17, 18, and 19. It can be seen that the load requirement is also met, operating most of the time in mode 1 and mode 3. Finally, the system is also evaluated with a more demanding load profile starting with $SOC_b^{init} = 80\%$ (Fig. 10, 21, and 22). It is remarkable that the hybrid system can meet the load all the time, including adverse periods when the wind-solar production is very low and the load is significantly greater.

As it was mentioned in Section 3, the main objectives in the design process are to achieve a reliable power supply under varying atmospheric conditions and minimize the total system cost. The results of this validation phase confirm that the first objective, consisting in $LPSP < LPSP_a$ with $LPSP_a = 2\%$, is satisfied in all test performed. In fact, the $LPSP$ values with the profiles used in the validation phase are much lower than the $LPSP_a$. This suggest that the cost of the system could be reduced with a reduced sizing. However, the implemented sizing is the result of an optimization procedure using a wide set of data along a year. This is because it may appear to be a more conservative design. A reduced design could be less expensive but at the expense of reduced robustness, reflected in a greater $LPSP$, in a more critical situation.

On the other hand, from the figures it can be seen that the wind and solar system are kept in nearly continuous operation, at maximum capacity. Which is why the load is mainly supported by these systems.

The battery makes an even more important job, meeting the high demands, or when environmental resources are too low. On the other hand, the PEM fuel cell is operated to supply the high demand periods and when the SOC_b is low, recovering it for its utilization a posteriori. From these observations it can be inferred that the wind-solar system is in charge of the short term operation, while the battery adjusts the delivered power in accordance with the demand. Moreover, the PEM fuel cell is in charge of securing the mid and long term sustainability of the system, maintaining the battery in adequate conditions, supplying the periods of bad weather conditions (including maintenance work), and fundamentally assuring the satisfaction of the demand when it is too high for the rest of the array.

6. Conclusions

Energy management for a stand-alone hybrid system that uses renewable energies (wind and solar) has been proposed. The inclusion of a PEM fuel cell, which is fed with hydrogen from a bioethanol reformer, to the wind-solar system provides a new concept to ensure a sustainable power supply for a wide range of atmospheric conditions. First, a methodology of optimal sizing using a GA approach was proposed. For this purpose, models of the wind turbines, the PV panels, the battery bank, the PEM fuel cell, and the bioethanol reformer (simplified model) were developed. Using these models, a procedure to achieve the optimal sizing of the hybrid system was proposed. The developed methodology is based on the use of long-term data of wind speed, solar radiation and ambient temperature in a particular location, and it has been applied to the design of a power system to supply a stand-alone household. Once designed the hybrid power system, the EMS has been developed.

The evaluation of the EMS performance is done using real weather data for the region of installation. Simulation results of the developed methodology indicate viability of the proposed energy management technique. Furthermore, the proposed methodology could be adapted to other stand-alone renewable systems. It it remarkable that the aggregation of the bioethanol processor allows to decrease the sizing of the other components, guaranteeing its operability even against adverse conditions. This is thanks to the inclusion of a chemical energy reserve that is environmentally friendly such as the bioethanol.

As future work a rigorous dynamic model of the closed-loop BRS connected with the wind-solar system will be considered. Then, a specific plant-wide control configuration will be designed.

References

Bajpai, P., Dash, V., 2012. Hybrid renewable energy systems for power generation in stand-alone applications: A review. Renewable and Sustainable Energy Reviews 16 (5), 2926–2939.

Basualdo, M., Feroldi, D., Outbib, R., 2011. PEM Fuel Cells with Bio-ethanol Processor Systems. Springer.

Bilodeau, A., Agbossou, K., 2006. Control analysis of renewable energy system with hydrogen storage for residential applications. Journal of Power Sources 162 (2), 757–764.

Borowy, B., Salameh, Z., 1996. Methodology for optimally sizing the combination of a battery bank and pv array in a wind/pv hybrid system. Energy Conversion, IEEE Transactions on 11 (2), 367–375.

Boukhezzar, B., Lupu, L., Siguerdidjane, H., Hand, M., 2007. Multivariable control strategy for variable speed, variable pitch wind turbines. Renewable Energy 32 (8), 1273–1287.

Boukhezzar, B., Siguerdidjane, H., 2005. Nonlinear control of variable speed wind turbines for power regulation. In: Control Applications, 2005. CCA 2005. Proceedings of 2005 IEEE Conference on. IEEE, pp. 114–119.

Campbell, G., Norman, J., 1998. An Introduction to Environmental Biophysics. Springer Verlag.

Chedid, R., Akiki, H., Rahman, S., 1998. A decision support technique for the design of hybrid solar-wind power systems. Energy Conversion, IEEE Transactions on 13 (1), 76–83.

Degliuomini, L. N., Feroldi, D., Basualdo, M., 2012a. Hydrogen production based on bio-ethanol and solar energy for feeding pem fuel cells. In: 20th Mediterranean Conference on Control and Automation (2012). pp. 1183–1188.

Degliuomini, L. N., Feroldi, D., Luppi, P., Basualdo, M., 2012b. Improvements on hydrogen production efficiency based on switching multiple renewable power sources. In: Elsevier (Ed.), Proceedings of the 22nd European Symposium on Computer Aided Process Engineering (2012). pp. 342–346.

Del Real, A., Arce, A., Bordons, C., 2009. Optimization strategy for element sizing in hybrid power systems. Journal of Power Sources 193 (1), 315–321.

Ekren, O., Ekren, B., 2008. Size optimization of a pv/wind hybrid energy conversion system with battery storage using response surface methodology. Applied Energy 85 (11), 1086–1101.

Erdinc, O., Uzunoglu, M., 2011. The importance of detailed data utilization on the performance evaluation of a grid-independent hybrid renewable energy system. International Journal of Hydrogen Energy 36 (20), 12664–12677.

Erdinc, O., Uzunoglu, M., 2012a. A new perspective in optimum sizing of hybrid renewable energy systems: Consideration of component performance degradation issue. International Journal of Hydrogen Energy.

Erdinc, O., Uzunoglu, M., 2012b. Optimum design of hybrid renewable energy systems: Overview of different approaches. Renewable and Sustainable Energy Reviews 16 (3), 1412–1425.

Eroglu, M., Dursun, E., Sevencan, S., Song, J., Yazici, S., Kilic, O., 2011. A mobile renewable house using pv/wind/fuel cell hybrid power system. International Journal of Hydrogen Energy 36 (13), 7985–7992.

Feroldi, D., Serra, M., Riera, J., 2009. Energy management strategies based on efficiency map for fuel cell hybrid vehicles. Journal of Power Sources 190 (2), 387–401.

Henson, W., 2008. Optimal battery/ultracapacitor storage combination. Journal of Power Sources 179 (1), 417–423.

HomerEnergy, September 2012. Energy modeling software for hybrid renewable energy systems. Available online, accessed on September 2012.

Hwang, J., Lai, L., Wu, W., Chang, W., 2009. Dynamic modeling of a photovoltaic hydrogen fuel cell hybrid system. International Journal of Hydrogen Energy 34 (23), 9531–9542.

Ipsakis, D., Voutetakis, S., Seferlis, P., Stergiopoulos, F., Elmasides, C., 2009. Power management strategies for a stand-alone power system using renewable energy sources and hydrogen storage. International Journal of Hydrogen Energy 34 (16), 7081–7095.

Johnson, V., 2002. Battery performance models in advisor. Journal of Power Sources 110 (2), 321–329.

Kellogg, W., Nehrir, M., Venkataramanan, G., Gerez, V., 1998. Generation unit sizing and cost analysis for stand-alone wind, photovoltaic, and hybrid wind/pv systems. Energy conversion, ieee transactions on 13 (1), 70–75.

Koutroulis, E., Kolokotsa, D., Potirakis, A., Kalaitzakis, K., 2006. Methodology for optimal sizing of stand-alone photovoltaic/wind-generator systems using genetic algorithms. Solar energy 80 (9), 1072–1088.

Larminie, J., Dicks, A., 2003. Fuel Cell Systems Explained, 2nd Edition. Wiley and Sons.

Lei, Y., Mullane, A., Lightbody, G., Yacamini, R., 2006. Modeling of the wind turbine with a doubly fed induction generator

for grid integration studies. IEEE Transaction of Energy Conversion 21 (1), 257–263.

Liu, X., Wang, P., Loh, P. C., Gao, F., Choo, F. H., 2010. Control of hybrid battery/ultra-capacitor energy storage for stand-alone photovoltaic system. In: Energy Conversion Congress and Exposition (ECCE), 2010 IEEE. IEEE, pp. 336–341.

Meteored, September 2012. Global climate, climatic data worldwide. Available online, accessed on September 2012.

Milocco, R., Castro, B., 2009. State of charge estimation in ni–mh rechargeable batteries. Journal of Power Sources 194 (1), 558–567.

Nehrir, M. H., Wang, C., Strunz, K., Aki, H., Ramakumar, R., Bing, J., Miao, Z., Salameh, Z., October 2011. A review of hybrid renewable/alternative energy systems for electric power generation: Configurations, control, and applications. IEEE Transactions on Sustainable Energy 2 (4), 392–403.

Nelson, D., Nehrir, M., Wang, C., 2006. Unit sizing and cost analysis of stand-alone hybrid wind/pv/fuel cell power generation systems. Renewable Energy 31 (10), 1641 – 1656.

Nieto, L., Biset, S., Luppi, P., Basualdo, M., 2011. A rigorous computational model for hydrogen production from bioethanol to feed a fuel cell stack. International Journal of Hydrogen Energy 37 (4), 3108–3129.

Pede, G., Iacobazzi, A., Passerini, S., Bobbio, A., Botto, G., 2004. FC vehicle hybridisation: an affordable solution for an energy-efficient FC powered drive train. J. of Power Sources 125 (2), 280–291.

Qi, A., Peppley, B., Karan, K., 2007. Integrated fuel processors for fuel cell application: A review. Fuel Processing Technology 88 (1), 3–22.

Qi, W., Liu, J., Chen, X., Christofides, P., 2011. Supervisory predictive control of standalone wind/solar energy generation systems. Control Systems Technology, IEEE Transactions on 19 (1), 199–207.

Rajkumar, R., Ramachandaramurthy, V., Yong, B., Chia, D., 2011. Techno-economical optimization of hybrid pv/wind/battery system using neuro-fuzzy. Energy.

Thounthong, P., Chunkag, V., Sethakul, P., Sikkabut, S., Pierfederici, S., Davat, B., 2011. Energy management of fuel cell/solar cell/supercapacitor hybrid power source. Journal of Power Sources 196 (1), 313–324.

Tsai, H., Tu, C., Su, Y., 2008. Development of generalized photovoltaic model using matlab/simulink. In: Proceedings of the World Congress on Engineering and Computer Science. Citeseer, pp. 846–851.

Valenciaga, F., Puleston, P., 2005. Supervisor control for a stand-alone hybrid generation system using wind and photovoltaic energy. Energy Conversion, IEEE Transactions on 20 (2), 398–405.

Valenciaga, F., Puleston, P., Battaiotto, P., nov 2001. Power control of a photovoltaic array in a hybrid electric generation system using sliding mode techniques. Control Theory and Applications, IEE Proceedings - 148 (6), 448–455.

Valenciaga, F., Puleston, P., Battaiotto, P., Mantz, R., 2000. Passivity/sliding mode control of a stand-alone hybrid generation system. IEE Proc. Control Theory Appl. 147 (6), 680–686.

Wang, C., Nehrir, M., 2008. Power management of a stand-alone wind/photovoltaic/fuel cell energy system. Energy Conversion, IEEE Transactions on 23 (3), 957–967.

Xu, D., Kang, L., Chang, L., Cao, B., 2005. Optimal sizing of standalone hybrid wind/pv power systems using genetic algorithms. In: Electrical and Computer Engineering, 2005. Canadian Conference on. IEEE, pp. 1722–1725.

Yang, H., Lu, L., Burnett, J., 2003. Weather data and probability analysis of hybrid photovoltaicwind power generation systems in hong kong. Renewable Energy 28 (11), 1813 – 1824.

Yang, H., Zhou, W., Lu, L., Fang, Z., 2008. Optimal sizing method for stand-alone hybrid solar–wind system with lpsp technology by using genetic algorithm. Solar energy 82 (4), 354–367.

Z'Graggen, A., Haueter, P., Maag, G., Romero, M., Steinfeld, A., 2008. Hydrogen production by steam-gasification of carbonaceous materials using concentrated solar energyiv. reactor experimentation with vacuum residue. International Journal of Hydrogen Energy 33 (2), 679–684.

Zhou, K., Ferreira, J., De Haan, S., 2008. Optimal energy management strategy and system sizing method for stand-alone

photovoltaic-hydrogen systems. International Journal of Hydrogen Energy 33 (2), 477–489.

Zhou, W., Lou, C., Li, Z., Lu, L., Yang, H., 2010. Current status of research on optimum sizing of stand-alone hybrid solarwind power generation systems. Applied Energy 87 (2), 380–389.

Table 1: Parameters used in the solar system

q	$1.6 \times 10^{-19}\, C$
A	1.6
K	$1.3805 \times 10^{-23}\, Nm\, K^{-1}$
K_l	$0.0017\, A\, ^{o}C^{-1}$
I_{or}	$2.0793 \times 10^{-6} A$
T_{ref}	$301.18\, K$
E_{go}	$1.10\, V$
C	$0.001\, F$
L	$0.004\, H$
n_p	20
n_s	1

Table 2: Parameters of the battery bank.

Parameter	Value
Type battery	Ni-MH
Total number of batteries	10
Nominal capacity of each battery	6 Ah
Nominal voltage	8 V
Maximum voltage	9 V
Minimum voltage	6 V

Table 3: Cost of the components in the hybrid system.

Component	Operation time (yr)	Initial cost (USD/kW)	Maintenance cost (USD/yr)	Replacement cost (USD/yr)
Solar system	25	6220	155	100
Wind system	15	4550	155	467
Batteries	5	90	67	445

Table 4: Optimal configuration of the hybrid system.

N_w	1
N_{PV}	20
$N_{b,\,s}$	10
$N_{b,\,p}$	1
$N_{b,\,T}$	10
N_{FC}	1

Table 5: Events in the set Σ.

Event	Description
1	$i_L^{req} > i_w^a$
2	$i_L^{req} < (i_w^a - \Delta i^{thr})$
3	$i_L^{req} > (i_w^a + i_{PV}^a)$
4	$i_L^{req} < (i_w^a + i_{PV}^a - \Delta i^{thr})$
5	$SOC_b \geq SOC_b^{max}$
6	$SOC_b \leq SOC_b^{min}$
7	$SOC_b < (SOC_b^{max} - \Delta SOC_b^{thr})$
8	$SOC_b > (SOC_b^{min} + \Delta SOC_b^{thr})$

Table 6: State/event table δ.

Current state	Event	Next state
s_1	5	s_4
	6	s_5
	1	s_2
s_2	5	s_4
	6	s_5
	2	s_1
	3	s_3
s_3	5	s_4
	6	s_5
	4	s_2
s_4	7	s_1
s_5	8	s_1

Table 7: Parameters used in the EMS validation.

Parameter	Description	Value
SOC_b^{min}	Minimum state of charge	20%
SOC_b^{max}	Maximum state of charge	90%
ΔSOC_b^{thr}	Threshold of the state of charge	20%
Δi^{thr}	Threshold of the load current	$15\,A$

Appendix A. Nomenclature

BRS	Bioethanol reformer system
CSTR	Continuously stirred tank reactors
EMS	Energy management stratrgy
ESR	Ethanol steam reformer
GA	Genetic algorithm
PEM	Polymer Electrolyte Membrane
PV	Photovoltaic
RES	Renewable Energy System
WGS	Water gas shift reactors
A	Swept blade area of the wind turbine $[m^2]$
A_c	Cell deviation from the ideal p-n junction characteristic
C	Capacitance $[C]$
C_{PV}	Initial cost of PV panels $[USD]$
C_b^*	Battery capacity $[Ah]$
C_C	Initial cost $[USD]$
C_f	Design constant of the blades
C_M	Maintenance cost $[USD]$
C_P	Efficiency of the turbine
C_R	Replacement cost $[USD]$
E	Energy $[Wh]$
E_{go}	Band-gap energy of the semiconductor used in the photovoltaic cell
I_{or}	Reverse saturation current at the reference temperature $[A]$
I_{ph}	Photovoltaic cell current under a given insolation $[A]$
I_{PV}	Photovoltaic current $[A]$
I_{sc}	Short-circuit photovoltaic cell current $[A]$
I_o	Current on the output terminal of the PV power converter $[A]$
I_{rs}	Photovoltaic cell reverse saturation current $[A]$
J	Cost functional
K	Boltzman constant $(1.3806488 \times 10^{-23}\ J\ K^{-1})$
K_l	Short-circuit current temperature coefficient
L	Inductance $[H]$
$LPSP$	Loss of power supply probability
$LPSP_a$	Allowed loss of power supply probability

$N_{b,\,p}$	Number of batteries in parallel
$N_{b,\,s}$	Number of batteries in series
N_b	Number of batteries
N_{FC}	Number of fuel cells
N_{PV}	Number of PV panels
N_w	Number of wind turbines
n_p	Number of PV cells in parallel
n_s	Number of PV cells in series
P	Power $[W]$
P/E	Power/Energy ratio
P_{FC}	Fuel cell power $[W]$
P_b	Battery power $[W]$
P_h	Heater power $[W]$
P_L	Load power $[W]$
P_w	Wind turbine power $[W]$
q	Charge of an electron ($-1.602176565 \times 10^{-19}\ C$)
r	Radius of the blades $[m]$
R_{int}	Battery internal resistance $[\Omega]$
S	Set of nodes in the statechart
s_0	Initial state in the statechart
SOC_b	Battery state of charge [%]
T	Temperature $[^oC]$
T_{ft}	Power failure time $[s]$
T_{op}	Operation time $[s]$
T_t	Total time $[s]$
u	Control signal of the PV power converter
v	Wind velocity $[m\ s^{-1}]$
V_{bus}	Bus voltage $[V]$
V_{oc}	Battery open circuit voltage $[V]$
V_b	Battery bank voltage $[V]$
$W_{H2,rct}$	rate of hydrogen reacted $[kg\ s^{-1}]$
β	Blade angle $[rad]$
ΔT	Sampling time $[s]$
δ	Function that maps states and input events to states in the statechart

λ	Tip speed ratio
ω_m	Speed angle of the turbine shaft $[rad\ s^{-1}]$
ρ	Penalization term
ρ_a	Air density (1.2 $kg\ m^3$)
ρ_p	Penalization term
Σ	Set of possible input events in the statechart
$\mathbf{x}$	Vector of decision variables

Subscripts and superscripts

av	Available
b	Battery
FC	Fuel cell
h	Heater
$init$	Initial
L	Load
lim	Limit
lw	Lower
max	Maximum
min	Minimum
nom	Nominal
PV	Photovoltaic
r	Rated
rct	Reacted
ref	Reference
req	Required
thr	Threshold
un	Unitary
u	Used
up	Upper
w	Wind

Figure captions

- Caption Figure 1: Schematic diagrame of the hybrid generation system from bioethanol.
- Caption Figure 2: Schematic diagram of the BRS.
- Caption Figure 3: Historical hourly data for optimal design - Solar radiation
- Caption Figure 4: Historical hourly data for optimal design - Wind speed
- Caption Figure 5: Historical hourly data for optimal design - Ambient temperature
- Caption Figure 6: Variation of cost during the GA optimization process
- Caption Figure 7: Schematic diagram of the energy management strategy based on state machine approach.
- Caption Figure 8: Average hourly temperature and insolation profile.
- Caption Figure 9: Average hourly wind profile.
- Caption Figure 10: Average hourly load demand
- Caption Figure 11: Simulation results (Test 1) - Power balance in the DC bus.
- Caption Figure 12: Simulation results (Test 1) - State of charge in the battery bank.
- Caption Figure 13: Simulation results (Test 1) - Operation mode.
- Caption Figure 14: Simulation results (Test 2) - Power balance in the DC bus.
- Caption Figure 15: Simulation results (Test 2) - State of charge in the battery bank.
- Caption Figure 16: Simulation results (Test 2) - Operation mode.
- Caption Figure 17: Simulation results (Test 3) - Power balance in the DC bus.
- Caption Figure 18: Simulation results (Test 3) - State of charge in the battery bank.
- Caption Figure 19: Simulation results (Test 3) - Operation mode.
- Caption Figure 20: Simulation results (Test 4) - Power balance in the DC bus.
- Caption Figure 21: Simulation results (Test 4) - State of charge in the battery bank.
- Caption Figure 22: Simulation results (Test 4) - Operation mode.